Two-Gap Superconductivity in $Ba_{1-x}K_xFe_2As_2$: A Complementary Study of the Magnetic Penetration Depth by Muon-Spin Rotation and Angle-Resolved Photoemission

R. Khasanov,[1,*] D. V. Evtushinsky,[2] A. Amato,[1] H.-H. Klauss,[3] H. Luetkens,[1] Ch. Niedermayer,[4] B. Büchner,[2] G. L. Sun,[5] C. T. Lin,[5] J. T. Park,[5] D. S. Inosov,[5] and V. Hinkov[5]

[1]*Laboratory for Muon Spin Spectroscopy, Paul Scherrer Institut, CH-5232 Villigen PSI, Switzerland*
[2]*Institute for Solid State Research, IFW Dresden, P.O. Box 270116, D-01171 Dresden, Germany*
[3]*IFP, TU Dresden, D-01069 Dresden, Germany*
[4]*Laboratory for Neutron Scattering, Paul Scherrer Institute and ETH Zürich, CH-5232 Villigen PSI, Switzerland*
[5]*Max-Planck-Institut für Festkörperforschung, Heisenbergstraße 1, 70569 Stuttgart, Germany*
(Received 15 January 2009; published 6 May 2009)

We investigate the magnetic penetration depth λ in superconducting $Ba_{1-x}K_xFe_2As_2$ ($T_c \simeq 32$ K) with muon-spin rotation (μSR) and angle-resolved photoemission (ARPES). Using μSR, we find the penetration-depth anisotropy $\gamma_\lambda = \lambda_c/\lambda_{ab}$ and the second-critical-field anisotropy $\gamma_{H_{c2}}$ to show an opposite T evolution below T_c. This dichotomy resembles the situation in the two-gap superconductor MgB_2. A two-gap scenario is also suggested by an inflection point in the in-plane penetration depth λ_{ab} around 7 K. The complementarity of μSR and ARPES allows us to pinpoint the values of the two gaps and to arrive to a remarkable agreement between the two techniques concerning the full T evolution of λ_{ab}. This provides further support for the described scenario and establishes ARPES as a tool to assess macroscopic properties of the superconducting condensate.

DOI: 10.1103/PhysRevLett.102.187005 PACS numbers: 74.70.−b, 74.25.Ha, 76.75.+i

Much effort is devoted to the investigation of the manifestations and mechanism of unconventional superconductivity in iron-arsenides, since many of their features clearly set them apart from other superconductors. *Ab initio* calculations, for instance, indicate that superconductivity originates in the d orbitals of the Fe ion, which normally would be expected to be pair breaking [1,2]. Several disconnected Fermi-surface sheets contribute to the superconductivity, as revealed by angle-resolved photoemission spectroscopy (ARPES) [3–6]. Furthermore, indication for multigap superconductivity was obtained in measurements of the first and second critical fields H_{c1} and H_{c2} [7,8], the magnetic penetration depth λ [9,10], as well as in point-contact Andreev reflection spectroscopy experiments [11].

Measurements of λ provide a conclusive method to reveal multigap superconductivity, since the presence of gaps with different gap-to-T_c ratios induces the appearance of inflection points in $\lambda(T)$ [12–15]. Measuring λ_i ($i = a$, b, or c) along certain crystallographic directions allows, in addition, the investigation of penetration-depth anisotropy γ_λ. Within the London approximation, which implies $\lambda_i^{-2} \propto n_s/m_i^*$ (n_s is the carrier concentration), γ_λ is directly related to the anisotropy of the supercarrier mass m^* via $\gamma_\lambda = \lambda_j/\lambda_i = \sqrt{m_j^*/m_i^*}$. As shown for the case of MgB_2 [16], a different temperature evolution of γ_λ and the second-critical-field anisotropy $\gamma_{H_{c2}}$ is also indicative of multigap superconductivity.

Here we report a combined study of the penetration depth in a single crystal of $Ba_{1-x}K_xFe_2As_2$ (BKFA) by means of μSR and ARPES. The sample was extensively characterized and several publications report its investigation by ARPES, magnetic neutron scattering, μSR, and magnetic force microscopy [5,6,17]. Resistivity and dc-susceptibility measurements demonstrate a sharp superconducting (SC) transition at $T_c = (32 \pm 1)$ K, reproducible among different crystals from the same growth batch, and x-ray powder diffraction has established the phase purity [17]. Most importantly for our study, the gap structure was investigated by ARPES [5]. Furthermore, the occurrence of electronic phase separation into antiferromagnetic (AF) and superconducting or normal state regions on a lateral scale of several tens of nanometers was established [5,17].

We begin by reporting on the μSR measurements which were carried out at the πM3 beam line at the Paul Scherrer Institute (Villigen, Switzerland). The $Ba_{1-x}K_xFe_2As_2$ single crystal with an approximate size of $5 \times 10 \times 0.06$ mm^3 was mounted on a holder specially designed to perform μSR measurements on thin single-crystalline samples. The transverse-field (TF) and the zero-field (ZF) μSR experiments were performed at temperatures ranging from 1.5 to 200 K. In two sets of TF measurements the magnetic field ($\mu_0 H = 10$ mT $> H_{c1}$) was applied in parallel and perpendicularly to the crystallographic c axis, respectively, and always perpendicularly to the muon-spin polarization. The typical counting statistics were $\sim 10^7$ positron events for each particular data point.

Experiments in transverse field allow us to study magnetic ordering as well as to obtain the superfluid density response [18]. Muons stopping in magnetically ordered parts of the sample lose their polarization relatively fast, since the magnetic field on the muon stopping site becomes a superposition of the external and the internal fields. The superconducting response is observed as an additional damping below T_c because of the inhomogeneous field distribution of the external field penetrating the sample in form of vortices. Our ZF μSR experiments reveal that the signal from the magnetically ordered parts vanishes within the first 0.3 μs. Bearing that in mind, in the whole temperature region the fit of TF data was restricted to times $t \geq 0.3$ μs (see Ref. [18] for details). For $T < T_c$, the TF μSR data were analyzed using the following two-component form:

$$A^{\mathrm{TF}}(t) = A_1 \exp(-(\sigma_{\mathrm{sc}}^2 + \sigma_{\mathrm{nm}}^2)t^2/2)\cos(\gamma B_1 t + \phi) + A_2 \exp(-\sigma_{\mathrm{nm}}^2 t^2/2)\cos(\gamma B_2 t + \phi). \quad (1)$$

Here A_1 and A_2 are the initial asymmetries of the first and the second component, $\gamma/2\pi = 135.5$ MHz/T is the muon gyromagnetic ratio, ϕ is the initial phase of the muon-spin ensemble, and the depolarization rates σ_{sc} and σ_{nm} characterize the damping due to the superconducting and the weak nuclear magnetic dipolar contributions, respectively. The second term on the right-hand side of Eq. (1) accounts for the parts of the sample remaining in the normal state [19]. Each set of TF μSR data, consisting of measurements in the $H \parallel c$ and $H \perp c$ configuration, respectively, was fitted simultaneously with A_1, σ_{nm}, ϕ, and B_2 as common parameters and σ_{sc}, B_1, and A_2 as individual parameters for each temperature point. The validity of our approach to fit some of the parameters globally was confirmed by examining the evolution of A_1, σ_{nm}, and B_2 in the "free" fit. Above T_c, the fit was simplified to the single Gaussian component only, with all parameters kept free. The results of the analysis are presented in Fig. 1.

The inset in Fig. 1 shows that the initial TF asymmetry $A^{\mathrm{TF}}(t=0) = A_1 + A_2$ (closed symbols) starts to decrease below $T \sim 70$ K, following the gradual enhancement of the magnetic fraction already investigated in this sample [17,20]. Here, we concentrate on the SC properties and study in detail the temperature range below T_c, which remained unexplored in the previous study [17]. We note that A^{TF} (closed symbols) and the asymmetry related to the superconducting fraction A_1 (dashed lines) are almost the same for the $H \parallel c$ and $H \perp c$ sets of measurements. This is exactly what is expected, since these asymmetries must represent the corresponding volume fractions (magnetic or superconducting).

The temperature evolution of the SC part of the muon-spin depolarization rate σ_{sc} is presented in the main panel of Fig. 1. It is worthwhile to note that in a homogenous superconductor σ_{sc} is expected to be proportional to the inverse squared magnetic penetration depth, $\sigma_{\mathrm{sc}} \propto \lambda^{-2}$. In addition, in single-crystalline sample the magnetic-field distribution in the superconductor in the mixed state is asymmetric and, therefore, cannot be described by a single Gaussian line (see, e.g., [13–15]). The $Ba_{1-x}K_xFe_2As_2$ sample studied here is, on the contrary, highly inhomogeneous [17], and the superconducting response, at our level of statistics, is well described by a single line of Gaussian

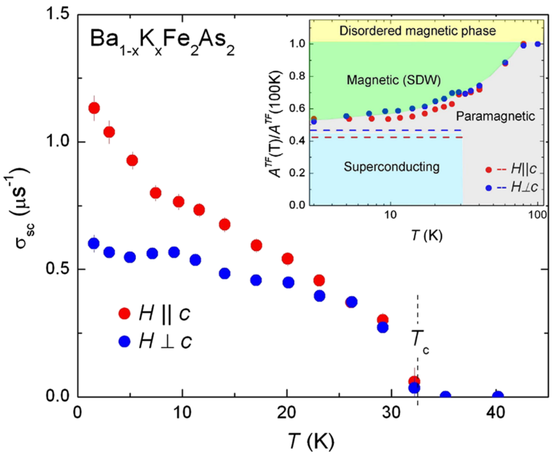

FIG. 1 (color online). Temperature evolution of σ_{sc} measured after field cooling in $\mu_0 H = 10$ mT applied in parallel (red or gray circles) and perpendicularly (blue or dark gray circles) to the crystallographic c axis. The inset shows the temperature evolution of the initial TF asymmetry $A^{\mathrm{TF}}(t=0) = A_1 + A_2$ (closed symbols) and the superconducting asymmetry A_1 (dashed lines) normalized to A^{TF} at $T = 100$ K. The colored or shaded areas represent volume fractions. Note the logarithmic T scale.

shape. We believe, however, that for $Ba_{1-x}K_xFe_2As_2$ σ_{sc} is still a good measure of λ. Indeed, σ_{sc} at $H \parallel c$ extrapolated to $T \to 0$ results in $\sigma_{\mathrm{sc}}(0) \simeq 1.2$ μs^{-1}, which follows reasonably well the Uemura relation established recently for various families of Fe-based superconductors [18,21]. We conjecture that the antiferromagnetic islands act as preformed pinning centers for vortices, thus precluding the formation of an ordered vortex lattice [17], while the screening current at this relatively low field ($\mu_0 H = 10$ mT) still flows at a distance λ from the vortex core.

Within the London model, the magnetic penetration depth of the isotropic extreme type-II superconductor ($\lambda \gg \xi$, ξ is the coherence length) is determined by $\lambda^{-2} \propto n_s/m^*$. For an anisotropic superconductor, the magnetic penetration depth is also anisotropic and is determined by an effective mass tensor [22]:

$$m^*_{\mathrm{eff}} = \begin{pmatrix} M_i & 0 & 0 \\ 0 & M_j & 0 \\ 0 & 0 & M_k \end{pmatrix}, \quad (2)$$

where $M_i = m_i^*/\sqrt[3]{m_i^* \cdot m_j^* \cdot m_k^*}$ and m_i^* is the mass of the carriers flowing along the ith principal axis. The effective penetration depth for the magnetic field applied along the ith principal axis of the effective mass tensor is then given by [22]:

$$\lambda_{\mathrm{eff}}^{-2} = \frac{1}{\lambda_j \lambda_k} \propto \frac{1}{\sqrt{m_j^* m_k^*}} \propto \sigma^{\| i}. \quad (3)$$

For convenience, we drop the index "sc" in the "superconducting" Gaussian relaxation rate σ_{sc}. Equation (3)

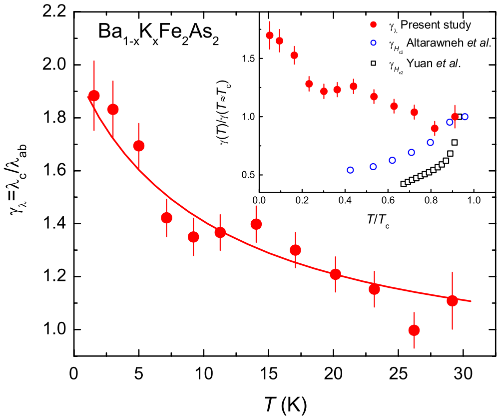

FIG. 2 (color online). Temperature evolution of the magnetic penetration-depth anisotropy $\gamma_\lambda = \lambda_c/\lambda_{ab} = \sigma^{\parallel c}/\sigma^{\perp c}$. The line is a guide to the eye. In the inset we compare γ_λ with the H_{c2}-anisotropy $\gamma_{H_{c2}}$ obtained for $Ba_{1-x}K_xFe_2As_2$ by Yuan *et al.* [23] and Altarawneh *et al.* [24], albeit in samples with somewhat different T_c. For better comparison, T is divided by the respective T_c and the values of γ_λ and $\gamma_{H_{c2}}$ are normalized to 1 for the data point closest to T_c.

implies that by applying the magnetic field along the crystallographic a, b, and c directions, one measures $\sigma^{\parallel a} \propto 1/\lambda_b\lambda_c$, $\sigma^{\parallel b} \propto 1/\lambda_a\lambda_c$ and $\sigma^{\parallel c} \propto 1/\lambda_a\lambda_b$, respectively. By neglecting the difference between λ_a and λ_b the penetration-depth anisotropy can be obtained as

$$\gamma_\lambda = \lambda_c/\lambda_{\rm ab} = \sigma^{\parallel c}/\sigma^{\perp c}. \tag{4}$$

The temperature evolution of γ_λ is presented in Fig. 2. The inset shows the second-critical-field anisotropy $\gamma_{H_{c2}} = H_{c2}^{\perp c}/H_{c2}^{\parallel c}$ obtained for similar $Ba_{1-x}K_xFe_2As_2$ samples in resistivity [23] and radio frequency penetration-depth measurements [24]. Within the phenomenological Ginzburg-Landau theory, in a single-gap superconductor both anisotropies must be equal [25]:

$$\gamma_\lambda = \frac{\lambda_c}{\lambda_{\rm ab}} = \sqrt{\frac{m_c^*}{m_{\rm ab}^*}} = \gamma_{H_{c2}} = \frac{H_{c2}^{\perp c}}{H_{c2}^{\parallel c}} = \frac{\xi_{\rm ab}}{\xi_c}. \tag{5}$$

It is natural to expect that the values of the same quantities measured by various techniques should be the same. While a deviation at a particular temperature might be explained by a slight variation of the properties among samples used in the different experiments, this cannot account for the opposite temperature evolution of γ_λ and $\gamma_{H_{c2}}$ shown in the inset of Fig. 2. Hence, in $Ba_{1-x}K_xFe_2As_2$ γ_λ and $\gamma_{H_{c2}}$ are not the same and Eq. (5) is violated. This resembles the situation in the two-gap superconductor MgB_2, albeit with reversed trends for γ_λ and $\gamma_{H_{c2}}$: In MgB_2, γ_λ was found to decrease with decreasing temperature from about 2 to 1.1, while $\gamma_{H_{c2}}$ increases from $\sim$2 at T_c to 6 at low temperatures [16]. It is worth noting that recently the presence of two distinct anisotropies γ_λ and $\gamma_{H_{c2}}$ was reported for the single-layer MFeAsO$_{1-x}$F$_x$ (M = Nd and Sm) [26] and the double-layer $BaFe_{2-x}Co_xAs_2$ [27]. The authors of Ref. [26] also explain the observed behavior by the presence of multiple gaps opening on various bands at the Fermi level.

An additional confirmation for the multigap behavior comes from the analysis of the temperature dependence of the in-plane magnetic penetration depth. Figure 3 shows $\lambda_{ab}^{-2}(T)$ obtained from the measured $\sigma^{\parallel c}(T)$ by using the relation $\sigma(\mu s^{-1}) = 0.1067\lambda^{-2}$ (μm^{-2}) [28]. The experimental $\lambda_{ab}^{-2}(T)$ data were analyzed within the framework of the phenomenological α model by assuming two independent contributions to the total λ_{ab}^{-2} [12]:

$$\lambda_{ab}^{-2}(T) = \lambda_{ab}^{-2}(0)(\omega\cdot\{1 - D[\Delta_1(T), T]\} + (1-\omega)\cdot\{1 - D[\Delta_2(T), T]\}), \tag{6}$$

where $D(\Delta, T) \equiv \int_{-\infty}^{+\infty}(-\frac{\partial f(\varepsilon)}{\partial\varepsilon}){\rm Re}\frac{\varepsilon}{\sqrt{\varepsilon^2-\Delta^2}}d\varepsilon$ [29], $f(\varepsilon)$ is the Fermi function, and ω is the contribution of the bigger gap to λ_{ab}^{-2}. The temperature dependence of the superconducting gap is assumed to be [12]

$$\Delta_{1,2}(T) = \Delta_{1,2}(0)\tanh\{1.82[1.018(T_c/T - 1)]^{0.51}\}, \tag{7}$$

in agreement with $\Delta(T)$ measured by ARPES [see Fig. 3(c)]. The solid line in Fig. 3(a) represents the result of a fit of Eq. (6) to the experimental data with $\lambda_{ab}(0)$, ω, Δ_1, and Δ_2 as free parameters. The fit yields Δ_1 = 9.1 meV, Δ_2 = 1.5 meV, ω = 0.5, and $\lambda_{ab}(0)$ = 320 nm [30].

The penetration depth $\lambda_{ab}(T)$ can also be calculated from the electronic band dispersion and the momentum-resolved SC gap [31] which were determined by ARPES on BKFA single crystals from the same growth batch [5,6,29,32]. The Fermi surface consists of four different sheets—an inner Γ barrel, an X pocket, and blade-shaped

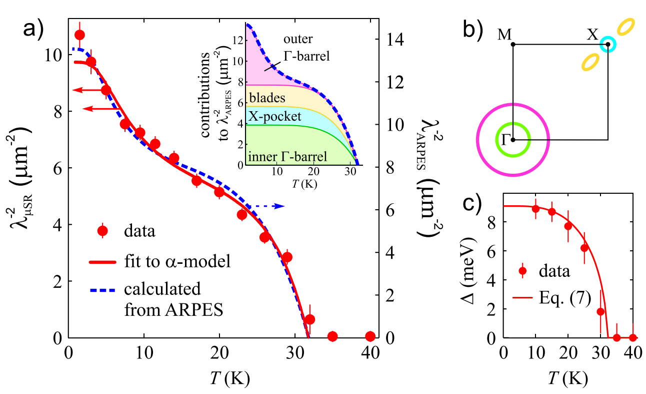

FIG. 3 (color online). Temperature evolution of the inverse squared in-plane magnetic penetration depth λ_{ab}^{-2} obtained from the measured $\sigma^{\parallel c}$ presented in Fig. 1 by using the relation $\sigma(\mu s^{-1}) = 0.1067\lambda^{-2}$ (μm^{-2}) [28]. The solid line represents the result of a fit of Eq. (6) to the α model, the dashed line represents a calculation of λ_{ab}^{-2} from the electronic structure revealed by ARPES [29] with *one* fitting parameter, Δ_2. Inset: contributions of different Fermi-surface sheets to λ_{ab}^{-2}. (b) Fermi surface of BKFA. (c) Temperature dependence of the SC gap, extracted from ARPES spectra [5].

TABLE I. Parameters as extracted from the fit of μSR data and calculated from ARPES data.

	μSR	ARPES
$\lambda_{ab}(0)$ (nm)	320	270
ω	0.51	0.55
Δ_1 (meV)	9.1	9.1
Δ_2 (meV)	1.5	<4

pockets with a large isotropic gap Δ_1, and an outer Γ barrel with a small gap Δ_2 [6,32] [Fig. 3(b)]. The formula relating λ to the electronic structure reads [29]

$$\lambda_{ab}^{-2}(T) = I_1\{1 - D[\Delta_1(T), T]\} + I_2\{1 - D[\Delta_2(T), T]\}, \quad (8)$$

where $I_{1,2}$ are integrals over the Fermi surface contours

$$I_1 = \frac{e^2}{2\pi\varepsilon_0 c^2 h L_c} \int_{\text{outer }\Gamma,\text{ blades},X\text{ pocket}} v_{\mathrm{F}}(\mathbf{k}) dk,$$
$$I_2 = \frac{e^2}{2\pi\varepsilon_0 c^2 h L_c} \int_{\text{inner }\Gamma} v_{\mathrm{F}}(\mathbf{k}) dk, \quad (9)$$

ε_0, h, e, c are physical constants, L_c is the c-axis lattice parameter, and v_{F} is the Fermi velocity. Further details of the electronic structure and the calculation are given in Ref. [29]. Equation (8) is equivalent to Eq. (6) with $\lambda_{ab}^{-2}(0) = I_1 + I_2$ and $\omega = \frac{I_1}{I_1+I_2}$. Using Eq. (8), we calculate $\lambda_{ab}^{-2}(0)$ and ω, while Δ_1 is known from the ARPES measurements [5,6]. A comparison of these parameters determined by the two different methods is shown in Table I. Taking into account the complementarity of the methods, the agreement is remarkable and strengthens the validity of the obtained results. The discrepancy in $\lambda_{ab}(0)$ is well within the range of values obtained in different μSR experiments [10].

Now we can assess the remaining parameter Δ_2 by fitting Eq. (8) to the measured $\lambda_{ab}(T)$ normalized to $\lambda(0)$. In Fig. 3 the normalization is realized by scaling the $\lambda_{\mu\mathrm{SR}}^{-2}$ and $\lambda_{\mathrm{ARPES}}^{-2}$ axes accordingly. We obtain $\Delta_2 = 1.1$ meV, again in good agreement with the μSR result.

In summary, from μSR measurements on a single-crystalline sample of BKFA ($T_c \simeq 32$ K) we have determined the anisotropy of the magnetic-field penetration depth $\gamma_\lambda = \lambda_c/\lambda_{ab}$. The penetration-depth anisotropy increases with decreasing T from $\gamma_\lambda \simeq 1.1$ at $T \simeq T_c$ to $\gamma_\lambda \simeq 1.9$ at $T \simeq 1.7$ K, while the T evolution of the H_{c2} anisotropy $\gamma_{H_{c2}}$ shows an opposite trend [23,24]. This resembles very much the situation in double-gap MgB_2 where both anisotropies are equal at T_c, but evolve oppositely with T. The notion of two SC gaps is supported by the observation of an inflection point in λ_{ab} at $\sim$7 K. From a fit of λ_{ab}^{-2} to the phenomenological α model we obtain gap values of $\Delta_1 = 9.1$ meV and $\Delta_2 = 1.5$ meV. A comparison of $\lambda_{ab}^{-2}(T)$ measured by μSR with the one calculated from ARPES data shows a remarkable agreement between these two complementary approaches, lending further support to our conclusions and establishing ARPES as a tool to estimate λ_{ab}.

The μSR work was performed at the Swiss Muon Source (SμS), Paul Scherrer Institute (PSI, Switzerland). ARPES results were obtained at BESSY.

*Corresponding author.
rustem.khasanov@psi.ch

[1] C. Cao, P. J. Hirschfeld, and H.-P. Cheng, Phys. Rev. B **77**, 220506(R) (2008).
[2] D. J. Singh and M. H. Du, Phys. Rev. Lett. **100**, 237003 (2008).
[3] H. Ding *et al.*, Europhys. Lett. **83**, 47001 (2008).
[4] L. Zhao *et al.*, Chin. Phys. Lett. **25**, 4402 (2008).
[5] D. V. Evtushinsky *et al.*, Phys. Rev. B **79**, 054517 (2009).
[6] V. B. Zabolotnyy *et al.*, Nature (London) **457**, 569 (2009).
[7] C. Ren *et al.*, Phys. Rev. Lett. **101**, 257006 (2008).
[8] F. Hunte *et al.*, Nature (London) **453**, 903 (2008).
[9] L. Malone *et al.*, arXiv:0806.3908.
[10] M. Hiraishi *et al.*, J. Phys. Soc. Jpn. **78**, 023710 (2009).
[11] P. Szabo *et al.*, Phys. Rev. B **79**, 012503 (2009).
[12] A. Carrington and F. Manzano, Physica (Amsterdam) **385C**, 205 (2003).
[13] R. Khasanov *et al.*, Phys. Rev. Lett. **98**, 057007 (2007).
[14] R. Khasanov *et al.*, J. Supercond. Novel Magnetism **21**, 81 (2008).
[15] R. Khasanov *et al.*, Phys. Rev. Lett. **99**, 237601 (2007).
[16] M. Angst and R. Puzniak, in *Focus on Superconductivity*, edited by B. P. Martines (Nova Science Publishers, New York, 2004), pp. 1–49.
[17] J. T. Park *et al.*, Phys. Rev. Lett. **102**, 117006 (2009).
[18] T. Goko *et al.*, arXiv:0808.1425.
[19] The second term in Eq. (1) may also include the background contribution arising from the muons stopped outside the sample.
[20] The difference between $A^{\mathrm{TF}}(T)$ obtained in the present study to that reported in [17] is due to different normalization. Here $A^{\mathrm{TF}}(T)$ is normalized to A^{TF} ($T = 100$ K), while in Ref. [17] $A^{\mathrm{TF}}(T)$ is normalized to the maximum asymmetry ($\simeq$21%) at our experimental setup.
[21] H. Luetkens *et al.*, Phys. Rev. Lett. **101**, 097009 (2008); R. Khasanov *et al.*, Phys. Rev. B **78**, 092506 (2008); A. A. Aczel *et al.*, Phys. Rev. B **78**, 214503 (2008).
[22] S. L. Thiemann, Z. Radović, and V. G. Kogan, Phys. Rev. B **39**, 11 406 (1989).
[23] H. Q. Yuan *et al.*, Nature (London) **457**, 565 (2009).
[24] M. Altarawneh *et al.*, Phys. Rev. B **78**, 220505(R) (2008).
[25] V. G. Kogan, Phys. Rev. B **24**, 1572 (1981).
[26] S. Weyeneth *et al.*, J. Supercond. Novel Magnetism **22**, 347 (2009).
[27] M. A. Tanatar *et al.*, Phys. Rev. B **79**, 094507 (2009).
[28] E. H. Brandt, Phys. Rev. B **37**, R2349 (1988).
[29] D. V. Evtushinsky *et al.*, arXiv:0903.4362.
[30] We estimate the true overall uncertainty in the absolute gap values to be of the order of 0.5–1 meV.
[31] B. S. Chandrasekhar and D. Einzel, Ann. Phys. (Leipzig) **505**, 535 (1993).
[32] V. B. Zabolotnyy *et al.*, arXiv:0904.4337 [Physica C (Amsterdam) (to be published)].